Comparative metabolomics reveals how the severity of predation by the invasive insect Cydalima perspectalis modulates the metabolism re–orchestration of native Buxus sempervirens

Anne-Emmanuelle Hay, Catherine Deborde, Thomas Dussarrat, Annick Moing, Annie Millery, T. Hoang, David Touboul, Marjolaine Rey, Léo Ledru, Sébastien Ibanez, et al.

plant biology

Plant Biology ISSN 1435-8603

RESEARCH ARTICLE

Comparative metabolomics reveals how the severity of predation by the invasive insect *Cydalima perspectalis* modulates the metabolism re–orchestration of native *Buxus sempervirens*

A. E. Hay[1], C. Deborde[2,3], T. Dussarrat[2], A. Moing[2,3], A. Millery[4], T. P. T. Hoang[5], D. Touboul[5], M. Rey[1], L. Ledru[4], S. Ibanez[4], P. Pétriacq[2,3], C. Vanhaverbeke[6] & C. Gallet[4]

1 Université Claude Bernard Lyon 1, Laboratoire d'Ecologie Microbienne – CESN, UMR CNRS 5557, UMR INRAE 1418, VetAgro Sup, Villeurbanne, France
2 Université Bordeaux, INRAE, Biologie du Fruit et Pathologie, UMR 1332, Bordeaux, France
3 Bordeaux Metabolome, MetaboHUB, PHENOME–EMPHASIS, Bordeaux, France
4 Laboratoire d'Ecologie Alpine UMR CNRS 5553, Université Savoie Mont–Blanc, Université Grenoble Alpes, Grenoble, France
5 Université Paris–Saclay, CNRS, Institut de Chimie des Substances Naturelles, UPR 2301, Gif-sur-Yvette, France
6 Université Grenoble Alpes, CNRS, DPM, Grenoble, France

Keywords
Boxwood; LC–HRMS; NMR; plant–insect relationships; quaternary ammonium compounds; specialized metabolites.

Correspondence
C. Gallet, Laboratoire d'Ecologie Alpine UMR CNRS 5553, Université Savoie Mont–Blanc, Université Grenoble Alpes, Chambéry–Grenoble F-73000, France.
E-mail: christiane.gallet@univ-smb.fr

Present address
INRAE, UR BIA, Biopolymers Interactions Assemblies, Nantes, France
INRAE, BIBS Facility, PROBE Infrastructure, Nantes Cedex, France

Editor
S.B. Unsicker

Received: 22 April 2024;
Accepted: 14 June 2024

doi:10.1111/plb.13691

ABSTRACT

- The recent biological invasion of box tree moth *Cydalima perspectalis* on *Buxus* trees has a major impact on European boxwood stands through severe defoliation. This can hinder further regrowth and threaten survival of populations.
- In a mesocosm approach and controlled larval density over a 2-month period, responses of *B. sempervirens* essential and specialized metabolites were characterized using metabolomics, combining ^{1}H–NMR and LC–MS/MS approaches. This is the first metabolome depiction of major *Buxus* responses to boxwood moth invasion.
- Under severe predation, remaining green leaves accumulate free amino acids (with the noticeable exception of proline). The leaf trans-4-hydroxystachydrine and stachydrine reached 10–13% and 2–3% (DW), while root content was lower but also modulated by predation level. Larval predation promoted triterpenoid and (steroidal) alkaloid synthesis and diversification, while flavonoids did not seem to have a relevant role in *Buxus* resistance.
- Our results reveal the concomitant responses of central and specialized metabolism, in relation to severity of predation. They also confirm the potential of metabolic profiling using ^{1}H–NMR and LC–MS to detect re-orchestration of metabolism of native boxwood after severe herbivorous predation by the invasive box-tree moth, and thus their relevance for plant–insect relationships and ecometabolomics.

INTRODUCTION

Biological invasions can lead to rapid and brutal suppression of native species (Brockerhoff & Liebhold 2017). A growing number of studies have reported that accidental or deliberate introduction of non-native species leads to outbreaks of populations. Such dramatic events are particularly described for plant–insect relationships, whether in agricultural systems or (semi)-natural forests (Kenis *et al.* 2009). In the latter, extensive or total defoliation of the tree can kill the whole individual and, at a larger scale, replace one species with another. In this scenario, no control of an invasive pest can overwhelm plant defences, which become ineffective in stopping or limiting the pest attack (Davidson *et al.* 1999).

A typical recent example is that between the common European box (*Buxus sempervirens L.*) and the invasive box-tree moth (*Cydalima perspectalis*, Lepidoptera: Crambidae; Walker 1859) in Europe. This insect first arrived and established in Germany in 2006/2007 (Van der Straten & Muus 2010) *via* the boxwood trade from Asia (Van der Straten & Muus 2010; Kenis *et al.* 2013; Bras *et al.* 2019). This moth is a herbivore of boxwood species (Leuthardt & Baur 2013), causing dramatic damage to the common European boxwood, *B. sempervirens*, the Caucasus *B. colchica* and rarer European species such as *B. balearica* (Kenis *et al.* 2013). Those moths rapidly spread throughout Europe, invading almost the entire European *Buxus* range and ravaging both ornamental and wild European box species (Bras *et al.* 2019). Moth fecundity is high, and individuals lay masses

of eggs directly on box leaves, allowing efficient feeding by larvae. After partial or entire defoliation, box can either grow back or die if the defoliation is recurrent or the bark is consumed (Kenis *et al.* 2013). Potential European natural enemies of this moth do not significantly alter invasive moth population dynamics (Kenis *et al.* 2013; Leuthardt & Baur 2013), and its impact may have significant economic and ecological consequences in the long term (Mitchell *et al.* 2018).

Buxus is an evergreen, slow-growing genus of small trees or a tall understorey plant with morphological and physiological plasticity (Letts *et al.* 2012). *Buxus* is cold- and drought-tolerant and could be used to ensure soil stability and water quality as it can grow on steep slopes. Invasion of *Cydalima* is as an added threat to natural boxwood stands, which have already undergone major declines (Di Domenico *et al.* 2012) caused by other pests, such as the fungus *Calonectria pseudonaviculata* (Mitchell *et al.* 2018).

Dynamics and consequences of plant–insect interactions on both species survival and ecosystem processes are closely controlled by specific traits of both partners. Survival of *Buxus* shrubs and trees after moth invasion first depends on their resistance to larval predation and second on re-sprouting ability following severe or total defoliation. Plant immune responses combine physical, constitutive and induced chemical traits to defend against herbivores (Erb & Reymond 2019). The leaf cuticle of *Buxus* is not an efficient barrier to larval grazing. Some chemical defences of the Buxaceae have been described in traditional folk medicine. Alkaloids are most important in *Buxus* species, with more than 100 identified in this family (Devkota *et al.* 2008; Zhang *et al.* 2015), including triterpenoid and steroid alkaloids with antibacterial, antimalarial and anti-acetylcholinesterase activity (Zhang *et al.* 2015; Szabó *et al.* 2021a). More specifically, *B. sempervirens* leaves contain at least 25 nor-triterpene alkaloids (Szabó *et al.* 2021b). Other specialized compounds in *Buxus* leaves include flavonoids and phenolic acids (Bernal *et al.* 2013). Nevertheless, further studies are necessary to elucidate the significance and ecological functions of these compounds in defence against herbivores. This is essential in the context of severe herbivory, which affects plant synthesis of specialized compounds, resource allocation between above- and belowground parts and its ability to regrow.

Metabolomics addresses questions related to plant responses to their environment and is a valuable and powerful tool (Barah & Bones 2015; Allwood *et al.* 2021; Anzano *et al.* 2022) that can reveal complex mechanisms that occur during plant–insect interactions; from recognition mechanisms between insect and host, to systemic responses in plant tissues (Maag *et al.* 2015; Dyer *et al.* 2018; Macel & Van Dam 2018). Comparative descriptions of plant metabolomes with and without pests have led to discovery of new active compounds in plant resistance (Sanchez-Arcos *et al.* 2019; Müller *et al.* 2024). Such studies have revealed that plant resistance depends on many chemicals rather than on a particular compound (Lopez-Goldar *et al.* 2018). In this context, we used a strategy where predation pressure was controlled to allow evaluation of the extent of *Buxus* response.

Here, we employed a semi-controlled system that reduced the chemical (both genetic and environmental) diversity of *B. sempervirens* metabolic products and controlled *Cydalima* predation pressure over its 2-month life cycle. We then characterized the metabolic shifts in leaves and roots using multi-platform metabolomics. We combined targeted analysis of free amino acids using liquid chromatography (LC), proton nuclear magnetic resonance (^{1}H–NMR) profiling for central metabolism analysis, and LC coupled with tandem mass spectrometry (LC–MS/MS) fingerprinting to characterize specialized metabolites. Using a gradient of larval pressure, from no to over-predation, we addressed the following questions regarding expected changes in *B. sempervirens*: (i) are nitrogen-containing compounds and other metabolites implicated in modified resource allocation strategy after predation; (ii) are specialized defence compounds differentially accumulated; and (iii) are the metabolic modifications induced by foliar predation controlled by intensity of predation pressure?

MATERIAL AND METHODS

Plant material and data analyses

To reduce natural variation in plant metabolism, we compared closely related individuals growing in the same conditions. The box trees were from the same Botanic place (La Ravoire F-73490) and were free of chemical treatment. The mesocosm experiment started in 2018, 4 April to 29 May 29, at the University Savoie Mont-Blanc campus in an isolated grassy area (45°38′30.0″ N, 5°52′02.7″ E), with a similar clmate to nearby natural box stands from which larvae were collected just before the start of the experiment. A total of 32 box trees, about 30-cm high in 1 l pots were isolated in 1 m^3 mesh cages (insect-proof netting PE 22:30, 920 × 920; DIATEX, Saint-Genis Laval, France) to prevent movement of larvae between the trees. There were seven predation pressure values with different numbers of caterpillars per box tree, with four replicates each, and four controls without any larvae. A total of 1,437 caterpillars were used.

Predation pressure is the ratio of number of leaves needed by all larvae to fulfil their development cycle over number of available leaves. We used seven ranges [2.0; 1.0; 0.75; 0.5; 0.25; 0.13; 0.07] by precisely counting the number of leaves for each tree and a mean of 25 leaves needed per month for its larval cycle (see Ledru *et al.* 2022; Figure S1). Cages were only watered by natural precipitation, regularly inspected, and moths removed as soon as they hatched.

After approximately 2 months, remaining caterpillars were removed and plants harvested, divided into roots, stems, senescent leaves and intact green leaves without predation, air-dried at room temperature for 48 h and each plant part weighed. Roots and green leaves were then freeze-dried (Freeze dryer YR05190; Kalstein, Paris, France) and further stored at −18 °C prior to analysis. For each tree, freeze-dried plant material was homogenized to a fine powder in a mill with 2-mm stainless steel beads and vigorous shaking for 1 min (Retsch, Haan, Germany). Each sample contained tissues from one plant, and four biological replicates were made for each organ and herbivory level. At high herbivory pressure (>0.75), the number of whole green leaves without predation dramatically decreased (Fig. 1C, D) but remained sufficient for analysis.

A linear mixed model was built to test the effect of larval density on biomass of each plant part (Rpackage lmerTest; Kuznetsova *et al.* 2017). Fixed effects were larval density (log (x + 1) transformed) and plant part. The interaction between larval density and plant part on biomass was also included, to

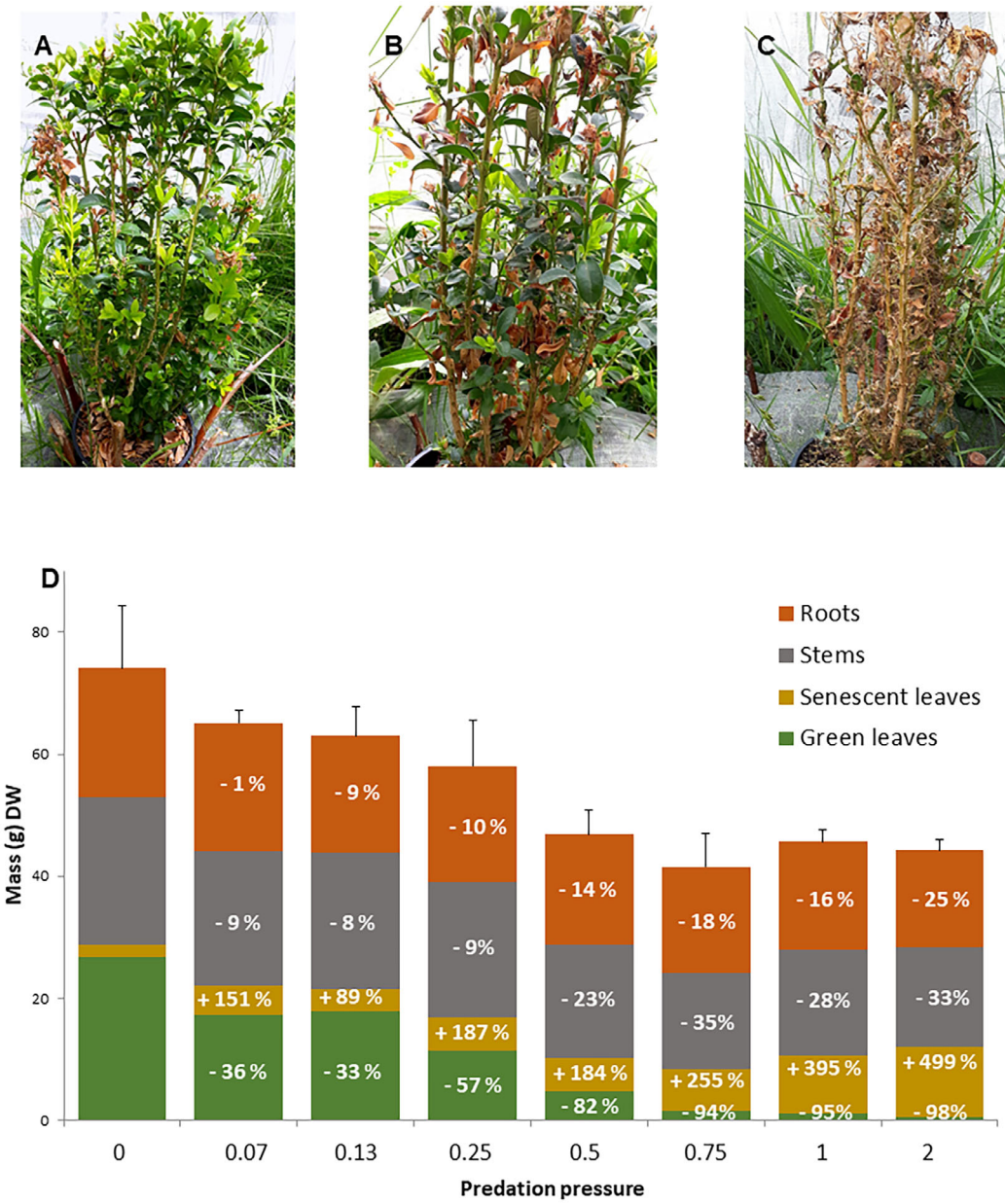

Fig. 1. Effect of predation by *C. perspectalis* on *Buxus sempervirens* saplings after 2 months. (A–C) Pictures of *B. sempervirens* shrubs after 2 months of predation at increasing larvae density (A) 0, (B) 0.13, (C) 0.5. Only three of the eight densities are shown. See text for further explanation of larvae density. (D) Plant biomass (total and for each plant compartment, g·DW). Values are mean of four replicates and upper bars are SD of total biomass (sum of the four compartments). Percentage (white letters) in middle of each column refers to magnitude of the effect of predation (compared to pressure = 0) on biomass.

test if the effect of larval density on biomass depends on the plant part (analysis of covariance, ANCOVA). Random effects were plant ID, since several measurements were made on each plant (one for each biomass part). Distribution of model residuals was visually checked and agreed with model assumptions of normality and homoscedasticity.

Central metabolism analyses

Amino acid analyses

For each lyophilized green leaf sample, 100 ± 2 mg DW was used for Polar extraction in 0.5 ml ethanol and water (70/30, v/v), by vortexing (Heidolph Top-mix 94323, Schwabach, Germany) and sonication (Bransonic Ultrasonic cleaner 2510E–DTH; Emerson, Saint-Louis, USA) for 10 min, followed by 5 min centrifugation at 20,000 *g* at room temperature. The resulting supernatants were dried under vacuum (CentriVap concentrator LABCONCO, Kansas City, USA), lyophilized (freeze dryer: YR05190, Kalstein) separated in two aliquots of about 20 mg (one for free amino acids the second for specialized metabolite determination) and weighed before storage at −20 °C until chromatographic analysis.

For LC-UV-Fluo analysis, the 32 lyophilized polar extracts were solubilized with norvaline (Nor, Agilent, Basel,

Switzerland) in pure water (100 μM), as internal standard, to a final concentration of extract of 20 $mg{\cdot}ml^{-1}$. Chromatographic analysis used high-pressure liquid chromatography (HPLC) (Agilent 1100; Agilent, Santa Clara, USA) with a guard cartridge and a C18 reverse phase column (Zorbax Eclipse– AAA 3.5 mm, 150 × 4.6 mm; Agilent Technologies) as previously described (Henderson *et al.* 2000). Nineteen proteogenic amino acids were detected and quantified: alanine (Ala), arginine (Arg), asparagine (Asn), aspartate (Asp), glutamine (Gln), glutamate (Glu), glycine (Gly), histidine (His), isoleucine (Ile), leucine (Leu), lysine (Lys), methionine (Met), phenylalanine (Phe), proline (Pro), serine (Ser), threonine (Thr), tryptophan (Trp), tyrosine (Tyr), and valine (Val) along with three non–amino acids: α-aminobutyric acid (α-ABA), citrulline (Cit), and γ-aminobutyric acid (GABA). Each response factor was determined using a 100 μM standard mix for each compound using ChemStation for LC 3D systems B01.03 (Agilent Technologies). Detection used UV at 338 nm for Asn and Nor. For each amino acid, absolute concentration (in μM) was calculated from UV or fluorescence chromatograms using Cabs = (CNor × Aabs)/(ANor × CR), where Cabs is amino acid absolute concentration, CNor norvaline concentration (μM), Aabs absolute area for amino acid, ANor absolute area for norvaline, and CR ratio between area of amino acid and norvaline.

Amino acid data analysis used MetaboAnalyst 5.0 (https://www.metaboanalyst.ca/, https://doi.org/10.1093/nar/gkab382, RRID:SCR_015539). The data (23 absolute concentrations) were first normalized (median normalization, cube root transformation, and Pareto scaling) before multi- and univariate statistical analyses. Principal components analysis (PCA) was performed. Dendrograms were built with filtered data (variable selection based on one-way ANOVAs for larvae density effect, $P < 0.05$ after correction for false discovery rate (FDR)), using Pearson distance and Ward's linkage rule on means per larval density for clustering.

^{1}H NMR-based metabolomics profiling

NMR-based metabolomic analyses of *B. sempervirens* green leaf and root samples were performed at the Bordeaux Metabolome Facility of MetaboHUB. Extraction and ^{1}H-NMR metabolomic profiling of semi-polar extracts was performed as described in Deborde *et al.* (2019). Lyophilized leaf and root powders (24 ± 1 mg DW) were extracted with deuterated solvents (50/50 v/v MeOD/deuterated phosphate buffer pH 6.0), and (trimethylsilyl)propionic–2,2,3,3–*d4* acid sodium salt (TSP) was used for chemical shift calibration. ^{1}H-NMR spectra were recorded at 500.162 MHz on a Bruker Avance III spectrometer (Bruker, Wissembourg, France) and using an ATMA broadband inverse 5-mm z-gradient probe flushed with nitrogen gas, at 300 K. A single-pulse sequence with presaturation (zgpr) was used. To optimize NMR conditions, automated tuning and matching, locking, shimming (topshim) and 90 ° hard pulse calibration (pulsecal) were carried out for each sample. The same dedicated receiver gain was used for all extracts of the same organ. 64 scans of 128 k data points each were acquired with a 90 ° pulse angle, a 7,000 Hz spectral width, a 9.35 s acquisition time, and a 10.64 s recycle delay. Each bucket was designated according to its central chemical shift value, in ppm. This resulted in 455 and 384 normalized (constant sum normalization, CSN) buckets with a signal-to-noise ratio (SNR) > 10 for the leaf dataset and the root dataset, respectively.

The confidence level of metabolite identification followed Sumner *et al.* (2007). ^{1}H-NMR peak assignments were based on chemical shifts, signal multiplicities, intensity ratios, comparison with NMR spectra of chemical standards (in-house database, dbrefMeOD@500) and chemical shift values from the BMRB database (BioMagResBank, www.bmrb.wisc.edu, RRID:SCR_002296) and literature. In addition, 1-D selective gradient experiments (COSY, NOESY, TOCSY), 1-D ^{13}C experiments and 2-D experiments, ^{1}H-^{1}H homonuclear correlated spectroscopy (COSY, TOCSY), ^{1}H-^{13}C heteronuclear single-quantum correlation (HSQC NUS) and ^{1}H-^{13}C heteronuclear multiple bond correlation (HMBC NUS) experiments were performed on selected samples to assist in annotation of ambiguous signals. One quantitative NMR spectrum of leaf extract (herbivory pressure 1) was acquired, with a 1-D single pulse sequence, a 90° pulse angle, a 14 ppm spectral width, 4.68 s acquisition time, 15 s recovery delay and 64 scans to quantify the major quaternary-ammonium metabolites. TSP was used as internal calibration standard. The correction factors for quantification of compounds from the NMR spectra with presaturation were then calculated for each specific compound and their content expressed in $mmol{\cdot}g^{-1}$ DW used for extraction or as percentage (m/m) DW. Apodisation (LB 0.2 Hz), zero-filling (X2) and Fourier transformation of Free Induction Decay, phasing, chemical shift calibration and local baseline correction were carried out with the NMRProcFlow web tool, www.nmrprocflow. Org, RRID:SCR_022777). Each spectral region of interest was determined manually with either intelligent bucketing (De Meyer *et al.* 2008) or variable size bucketing modules of NMRProcFlow.

The NMR data and metadata have been deposited in the recherche.data.gouv.fr repository (https://doi.org/10.57745/HX6NZL) for representative extracts of *B. sempervirens* root and leaf.

The NMR data analysis was performed using MetaboAnalyst 5.0. The CSN data (455 and 384 buckets, for leaves and roots, respectively) were first normalized (median normalization, cube root transformation, and Pareto scaling) before multi- and univariate statistical analyses. PCA was performed. Dendrograms and corresponding heatmaps were built using Pearson distance and Ward's linkage rule for clustering of filtered data (variable filtration based on one-way ANOVA for larvae density effect, $P < 0.01$ and 0.05 for leaves and roots, respectively, with FDR correction) using means per larval density to highlight significant trends.

Specialized metabolite LC–MS/MS-based analyses

To further assess specialized metabolites, we performed apolar (ethyl acetate (EtOAc)) extractions on green leaf lyophilized powder in addition to the polar extracts (also used for free amino acid determination). Similarly, 32 other lyophilized samples of green leaves were weighed (5 ± 2 mg DW) and extracted with 0.5 ml 100% EtOAc to obtain apolar extracts, dried under vacuum (CentriVap concentrator LABCONCO) precisely weighed before storage at −20 °C until LC–MS/MS analysis.

Each dried apolar extract was solubilized in 300 μl 100% EtOH (2.5 $mg{\cdot}ml^{-1}$ DW), and a 50 μl aliquot transferred into a vial for LC–MS/MS analysis. The remaining solutions were dried and stored at −20 °C until targeted analyses. LC–MS/MS experiments on polar and apolar extracts were performed with a 1260 Prime HPLC (Agilent Technologies, Waldbronn,

Germany) coupled with an Agilent 6540 Q–ToF tandem mass spectrometer. LC separation was achieved on an Accucore RP–MS column (100 × 2.1 mm, 2.6 μm; Thermo Scientific, Les Ulis, France) with a mobile phase consisting of H_2O/formic acid (99.9/0.1 v/v) (A) – acetonitrile/formic acid (99.9/0.1) (B). The column oven was set at 45 °C. Compounds were eluted at a flow rate of 0.4 ml·min^{-1} with a gradient from 5% to 100% B in 20 min, then 100% B for 3 min. The injection volume was fixed at 5 μl for all analyses. Mass spectra were recorded in electrospray positive ionization mode with the following parameters: gas temperature 325 °C, drying gas flow rate 10 l·min^{-1}, nebuliser pressure 30 psi, sheath gas temperature 350°C, sheath gas flow rate 10 l·min^{-1}, capillary voltage 3,500 V, nozzle voltage 500 V, fragmentor voltage 130 V, skimmer voltage 45 V, octopole 1 RF voltage 750 V. Internal calibration was achieved with purine and hexakis (1H, 1H, 3H tetrafluoropropoxy)phosphazene (*m/z* 121.0509 and *m/z* 922.0098), providing mass accuracy >5 ppm. The data-dependent MS/MS events were acquired for the five most intense ions detected by full-MS, in the *m/z* range 100–1,700, above an absolute threshold of 1,000 counts. Selected precursor ions were fragmented at a fixed collision energy of 30 eV and with an isolation window of 1.3 amu. The mass range for MS/MS analysis was set as *m/z* 50–1,500.

The data files were converted from .d standard data format (Agilent Technologies) to .mzXML format using MSConvert software (ProteoWizard package 3.0; https://doi.org/10.1038/nbt.2377, RRID:SCR_012056). All .mzXML values were processed using MZmine 2.53 as described by Olivon *et al.* (2017). Mass detection was performed with an MS1 noise level of 1,000 and an MS/MS noise level of 500. The ADAP chromatogram builder was employed with a minimum group size of 4 scans, group intensity threshold of 3,000, minimum highest intensity of 8,000 and *m/z* tolerance of 0.08 (or 20 ppm). Deconvolution was performed with the ADAP wavelet algorithm with the following settings: SNR threshold = 10, minimum feature height = 5,000, coefficient/area threshold = 10, peak duration range 0.00–0.4 min and t_R wavelet range 0.00–0.1 min. MS/MS scans were paired using a *m/z* tolerance range of 0.01 Da and t_R tolerance range of 0.4 min. Isotopologs were grouped using the isotopic peak grouper algorithm with a *m/z* tolerance of 0.08 (or 20 ppm) and a t_R tolerance of 0.2 min. Peaks were filtered using a feature list row filter, keeping only peaks with MS/MS scans. Peak alignment was performed using the join aligner with a *m/z* tolerance of 0.008 (or 20 ppm), a weight for *m/z* at 75, a retention time tolerance of 0.2 min and weight for t_R at 25. The MGF file and the metadata were generated using the export/submit to GNPS option (RRID:SCR_019012).

First, to test effect of larval density on number of polar and non-polar features, a linear mixed model was built (Rpackages lmerTest and emmeans; Lenth 2022)). Fixed effects correspond to larval density (log(x + 1) transformed) and to feature type (polar or non-polar). The interaction between larval density and feature type on feature abundance was included to test whether the effect of larval density on abundance depends on polarity (ANCOVA). Random effects corresponded to plant ID since two extracts are made from each plant. The distribution of the model residuals agreed with model assumptions of normality and homoscedasticity (visual check).

Molecular networks were calculated and visualized using MetGem 1.3 (https://doi.org/10.1021/acs.analchem.8b03099). MS/MS spectra were window-filtered by choosing only the top six peaks in the ±50 Da window throughout the spectrum. All fragment ions in the ±17 Da range around the precursor *m/z* were removed. The *m/z* tolerance windows used to find the matching peaks were set to 0.02 Da, and cosine scores (minimal cosine score 0.7) were kept in consideration for spectra sharing at least two matching peaks. MS/MS data annotations were performed in two steps: a search of standards (*m/z* error at 0.02 Da) and a search of analogues (±200 Da). Only results with cosine scores >0.9 and 0.7 were considered for standards and analogues, respectively.

Figures for molecular networks were generated using MetGem export function and ChemDraw Professional 16.0 (PerkinElmer, Waltham, MA, USA) https://doi.org/10.5281/zenodo.8263903.

The LC–MS/MS quantification data were analysed using MetaboAnalyst 5.0. The data (1,606 and 1,311 *m/z* features for both extracts, respectively) were first normalized (median normalization, cube root transformation, and Pareto scaling) before multi- and univariate statistical analyses. A PCA was conducted for polar and apolar data separately to obtain an overview of the data. Clustering dendrograms (distance measure using Pearson's correlation, and clustering using Ward algorithm) and corresponding heatmaps were built with filtered data (variable filtration based on one-way ANOVAs for larvae density effect, $P < 0.01$ with FDR correction) using means per larvae density to highlight significant trends. We adopted sparse Partial Least Square Discriminant Analysis (sPLS–DA) as a supervised method for predictive and descriptive modelling with discriminative variable selection (https://bmcbioinformatics.biomedcentral.com/articles/10.1186/1471-2105-12-253). The 100 most relevant variables selected by the sPLS–DA for the first latent variable (LV1, loadings values) were collected for both LC/MS–MS datasets and added to the 100 most significant variables according to the one-way ANOVA for larval density effect ($P < 0.01$ FDR corrected). After removing redundant variables between the LC–MS/MS data sets, a list of 208 relevant features was obtained.

RESULTS

Larvae predation affects box aspect and biomass

As expected, a visual observation of *B. sempervirens* shrubs revealed drastic effects of larvae occurrence on the aerial part (Fig. 1A–C). Biomass comparisons confirmed that leaf predation had deleterious effects on above- and belowground biomass, with increasing impacts according to larval density (Fig. 1D). The biomass of green leaves drastically decreased ($P < 0.0001$), and senescent leaves outnumbered green leaves for densities >0.5. Larval density also significantly decreased stem ($P < 0.0001$) and root ($P = 0.011$) biomass and increased senescent leaf ($P < 0.0001$) biomass. The negative effect of larval density was stronger for green leaves than for roots or stems ($P < 0.0001$ in both cases) and similar between roots and stems ($P = 0.51$).

Larvae predation modifies the amino acid profile of green leaves

For metabolites of central metabolic pathways, we first scored free amino acids in green leaves because of their central role in development of both boxwood and larvae. In the absence of

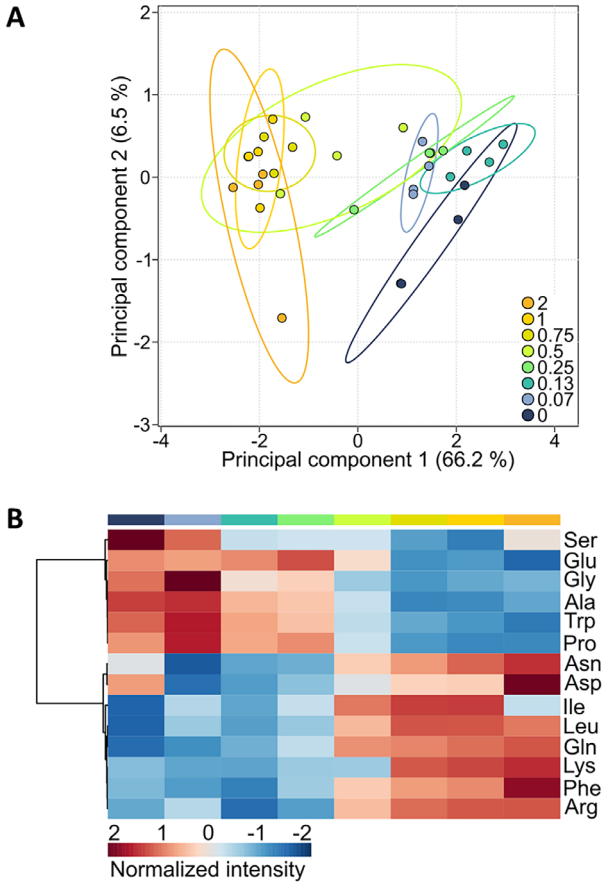

Fig. 2. PCA and clustering analysis of free amino acid content (LC-UV) in green leaves of *Buxus sempervirens* at eight larvae densities, from dark blue (0) to orange (2). (A) PCA plot for the first two components (PC1 and PC2) showing changes in 19 amino acids in 32 leaf samples. Ellipses represent 95% confidence interval. (B) Heatmap of a double clustering analysis for 14 amino acids whose concentrations vary significantly (ANOVA, $P < 0.05$, FDR corrected) across eight larvae density treatments. Each row represents an amino acid and each column a larvae density. The map was constructed using Pearson distance and Ward's linkage rule on means per larval density and after Pareto scaling. Higher than average (mean centred) values are in red, lower values are in blue.

larvae, 19 amino acids or relatives were detected, Pro being most abundant (41 µmol·g^{-1} DW), followed by Ala, Asn, GABA, Trp, Val, Ser (1–8 µmol·g^{-1} DW). PCA revealed a progressive shift in amino acid profiles according to larvae density, mainly on PC1 axis (66.2% of total variance; Fig. 2A). This trend was confirmed by univariate analyses and clustering analysis, showing that the content of 14 amino acids varied significantly across density treatments (Fig. 2B). Leaf content of Pro slightly increased between the 0 and 0.25 larval pressure but decreased at further larval densities. In contrast, concentrations of other amino acids, including Asn, increased in response to predation. As a result, the total amino acid concentration (sum of the 19 amino acids) increased by a factor of 3.6 between plants without larvae and plants with a larval pressure of 2.0 (Figure S2). Both PCA and heatmap highlighted the density treatment 0.5 as the critical point where nitrogen metabolism changed drastically.

Larvae predation modifies relative content of central metabolites in green leaves and roots

To increase understanding of the response of central metabolism to herbivory, central metabolites were profiled for both green leaves and roots using ^{1}H–NMR (Fig. 3, Figure S3A, B). In green leaves, the dataset of 455 buckets comprised 20 identified metabolites (Table S1) and a range of unknown compounds. The identified compounds included organic (citric, formic, fumaric, malic, quinic) acids, soluble carbohydrates (glucose, sucrose), a polyol (inositol), and amino acids (Ala, Asn, Asp, Ile, Leu, Pro, Tyr, Val). For Pro quantification, there is good overlap between Pro absolute quantification by LC–UV (Figure S2) and relative quantification by ^{1}H–NMR (Fig. 4). Less common than amino acids, betaines or Quaternary Ammonium Compounds (QAC), i.e. N-containing compounds characterized by a quaternary ammonium (stachydrine or Pro-betaine, trans-4-hydroxystachydrine, choline and trigonelline) were also annotated (Figure S4) and quantified in one leaf sample under herbivory pressure 1.0. Trans-4-hydroxystachydrine was quantified from its characteristic methyl group (3 H) at 3.14 ppm, stachydrine from its characteristic methyl group (3 H) at 3.13 ppm, choline from its characteristic methyl group (9 H) at 3.21 ppm, and trigonelline from its characteristic methyl group (3 H) at 4.45 ppm. NMR quantification revealed trans-4-hydroxystachydrine as the most abundant QAC in leaf samples (14% DW), followed by stachydrine (3% DW), choline (0.2% DW) and trigonelline (0.1% DW). The content of trans-4-hydroxystachydrine and stachydrine were calculated with correction factors for the whole dataset. Trans-4-hydroxystachydrine reached a maximum of 10–13% DW and stachydrine 2–3% DW in leaves under herbivory pressures 1.0 or 2.0. In roots, the ^{1}H–NMR dataset of 384 buckets comprised 22 identified metabolites and a range of unknown compounds (Figure S4, Table S1). Metabolites included organic (formic, fumaric, malic, succinic) acids, soluble carbohydrates (glucose, fructose, trehalose and sucrose), amino acids (Ala, Asn, Asp, Pro, Tyr) and QAC metabolites (stachydrine, trans-4-hydroxystachydrine, choline and trigonelline). Trans-4-hydroxystachydrine reached a maximum of 1.2% DW and stachydrine of 2% DW in roots without herbivory.

For leaves, the PCA of ^{1}H–NMR profiles (Fig. 3A) revealed a clear compositional shift along PC1 (76% of total variance). Samples clustered into two groups: 0 to 0.25 larvae density on the negative side, and 0.75 to 2.0 larval density on the positive side of PC1. Samples of 0.5 larval density had an intermediate position. Discrimination of root sample groups was weaker according to a PCA of ^{1}H–NMR profiles, with a marked separation only between the highest and lowest larval densities (Figure S5A).

Univariate and clustering analyses confirmed that increasing larval density significantly modified the relative content of 342 buckets for leaves (Fig. 3B) and 141 buckets for roots (Figure S5B). For Pro, sucrose and glucose, the trend of a slight increase observed in relative foliar content under the lowest predation pressure rapidly reversed above the 0.5 predation level, and final content decreased 4-, 7- and 12-fold compared to controls, respectively (Fig. 4). A similar decrease in root relative content was observed for these metabolites (Fig. 4). Conversely, the QAC stachydrine, trans-4-hydroxystachydrine and

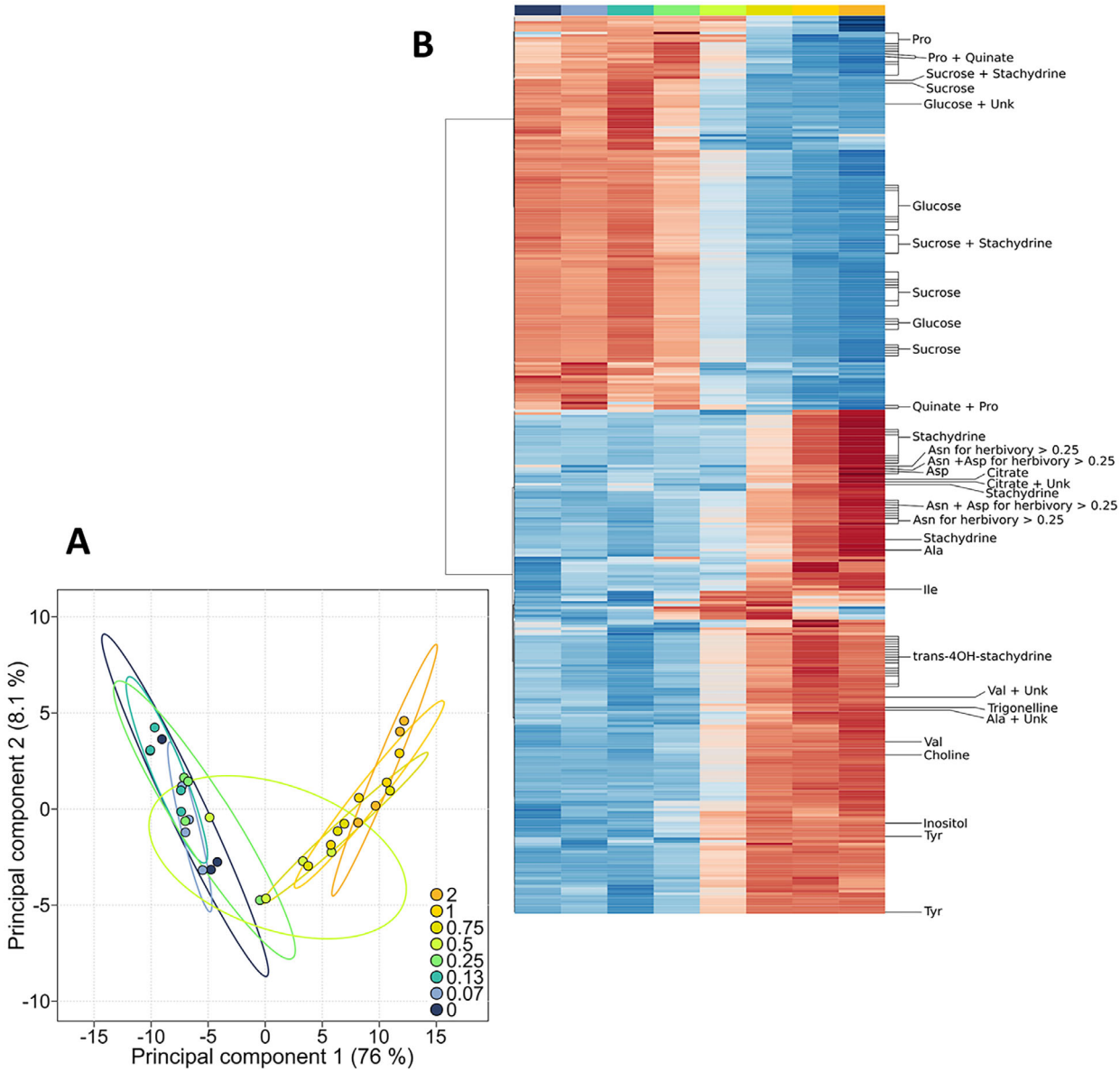

Fig. 3. PCA and clustering analysis of ^{1}H-NMR data in green leaves of *Buxus sempervirens* plants (central metabolism) with eight larvae densities, coloured from dark blue (0) to orange (2) and comparison of relative abundance of selected biomarkers. (A) PCA plot for the first two components (PC1 and PC2), based on 455 buckets in 32 leaf samples. (B) Heatmap of double clustering analysis for the 342 buckets whose concentrations vary significantly (ANOVA, $P < 0.01$, FDR corrected) across the eight ldensity treatments. Each row represents a bucket (with corresponding metabolite name when annotated) and each column a larval density. The map was constructed using Pearson-correlation distance and Ward's linkage rule on means per larval density and after Pareto scaling. Higher than average (mean-centred) values are in red, lower values are in blue. Unk = unknown.

choline accumulated under the highest predation pressure by a factor 2 to 3 in green leaves, without marked trends in roots (Fig. 4).

Specialized metabolites are also affected by larvae occurrence

To capture most *B. sempervirens* specialized metabolites, we deployed LC/MS–MS of polar and apolar extracts. Without predation polar extracts yielded more features than apolar ones (n = 1,564 vs n = 1,308 ; Figure S6). Features in apolar extracts were highest (n = 1,346) with 0.75 predation, representing a slight (+3%) but significant increase compared to the control.

The PCA (Figure 5A, B) revealed gradual shifts in specialized metabolites both for polar and apolar extracts along PC1 (respectively, 56.5% and 57.6% of total variance). A total of 1,004 and 972 features, respectively, from polar and apolar extracts responded significantly to predation pressure (Fig. 5C, D). For polar extracts (Fig. 5C), clear shifts in metabolism appeared as larval density increased, with a decisive split at the 0.5 level. The last column (2.0 predation) revealed exacerbated differences that could be attributed to drastic changes caused by plant collapse. The pattern from analysis of apolar extracts was quite similar (Fig. 5D).

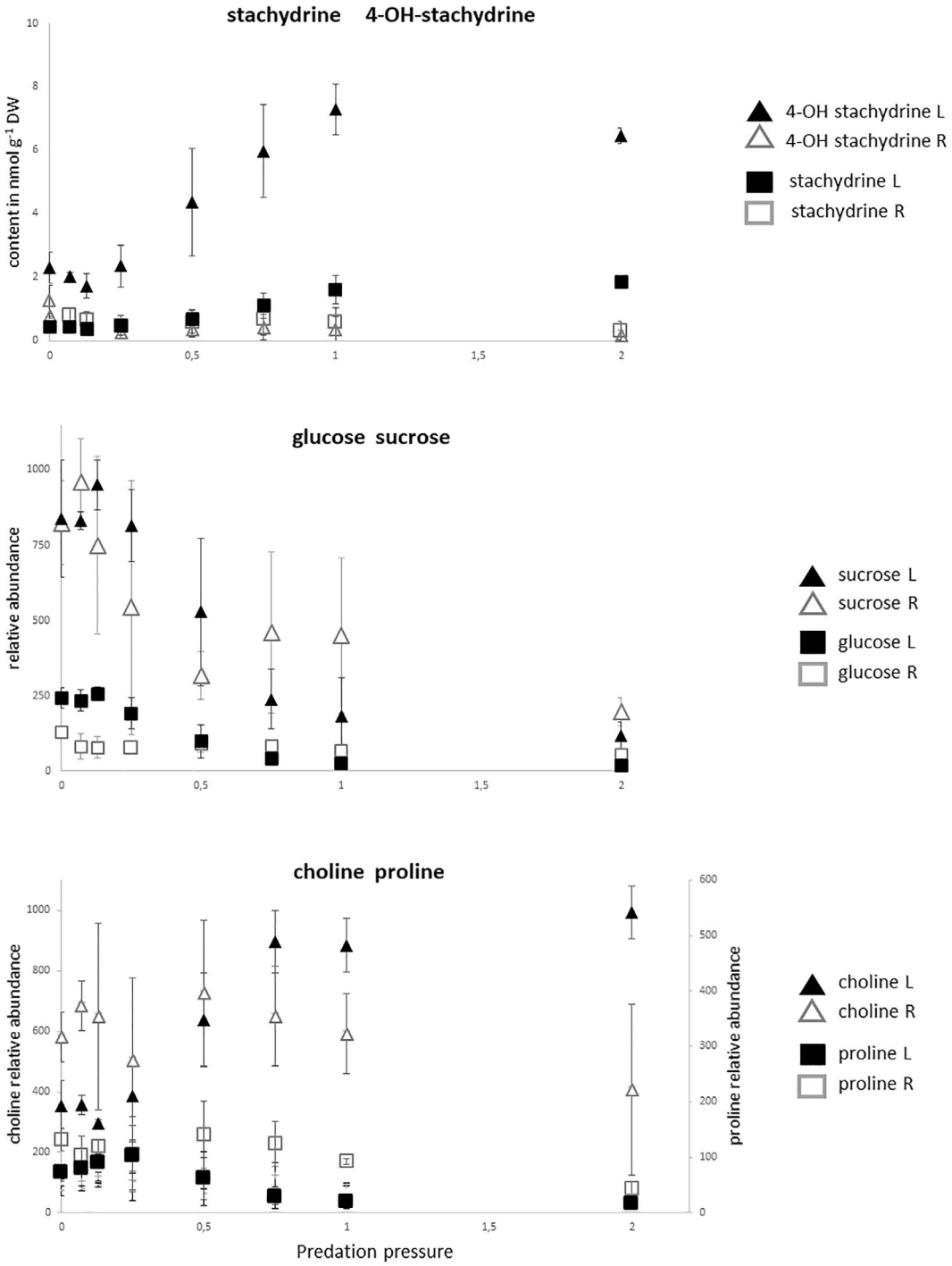

Fig. 4. Comparison of selected leaf (L) and root (R) biomarkers that are significantly modulated by predation pressure. Mean ± SD (n = 4) of content in nmol·g^{-1} DW for 4-OH-stachydrine and stachydrine; and relative abundance of corresponding buckets for sucrose, glucose, choline and proline.

(Steroidal) alkaloids are prominent biomarkers of box predation

To gain insights into the chemistry, the 100 most predictive variables selected by the sPLS–DA (first component) and the 100 most significant variables from both extracts (ANOVA, $P < 7.5 \times 10^{-7}$ apolar, 1.8×10^{-7} polar, FDR corrected) were collected and merged, yielding a total of 400 variables to annotate. After removing redundant relevant variables among the 400 of the two extract types, 208 relevant features (with m/z–t_R couple) was obtained (Table S2). Molecular networks were only surveyed for relevant variables using ANOVA and sPLS–DA. The proposed molecular formula (Metlin) was further confirmed from databases (ChEBI, RRID:SCR_002088; DNP, https://www.chemnetbase.com/) and literature.

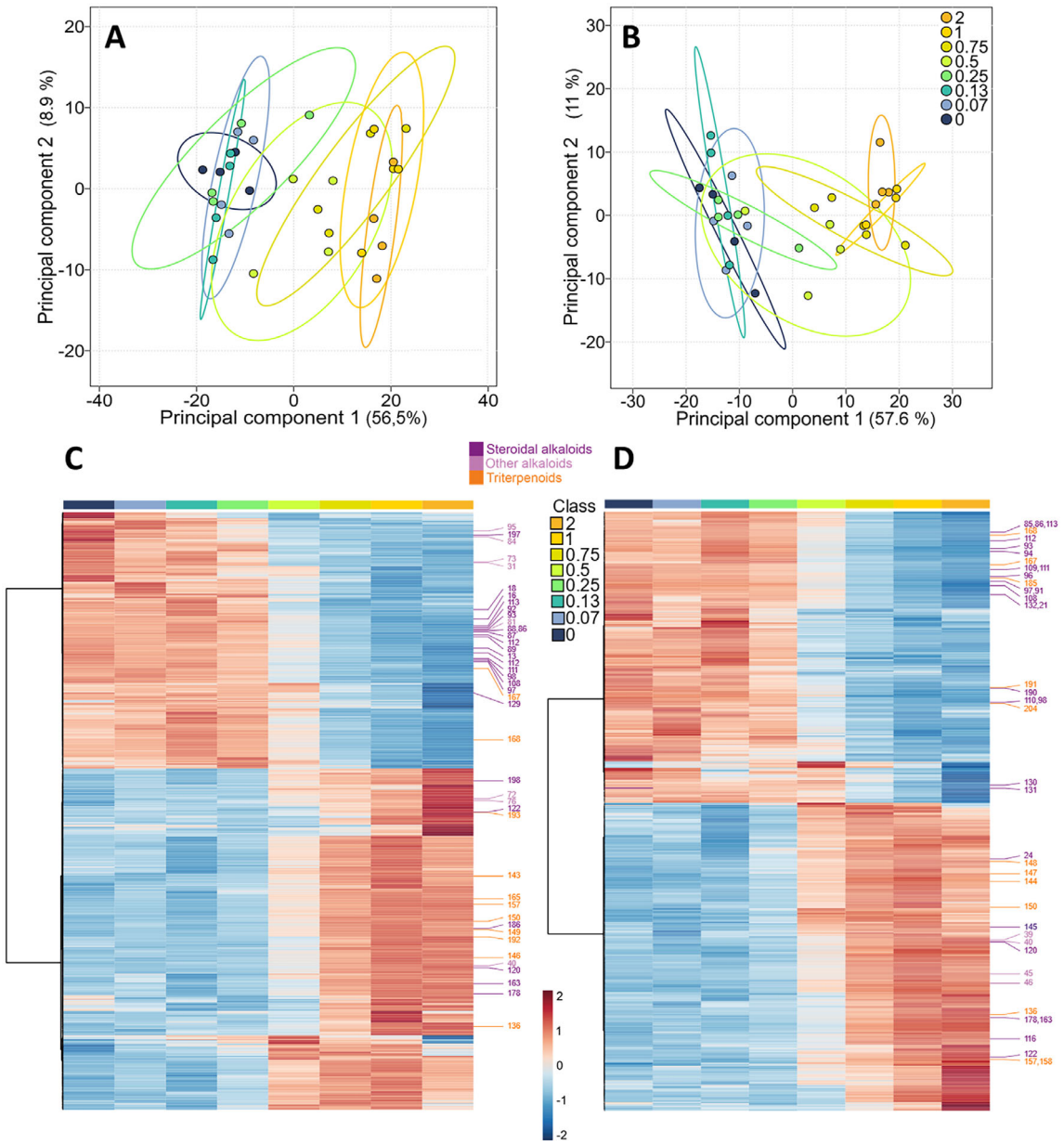

Fig. 5. PCA and clustering analysis of LC–MS/MS data in green leaves of *Buxus sempervirens* (specialized metabolism) with eight larval densities from dark blue (0) to orange (2). (A, B) PCA scores plot for first two components (PC1 and PC2) based on LC-MS data showing changes in metabolite features from polar (A) and apolar (B) extracts (1605 and 1391, respectively) of 32 samples of *B. sempervirens* green leaves with different larval densities. (C, D) Heatmap of double clustering analysis for 1004 and 972 features of polar (C) and apolar (D) extracts, respectively, whose concentrations vary significantly (ANOVA, $P < 0.01$, FDR corrected) along the eight larval density treatments. Each row represents a metabolite signature and each column a larvae density. Number refers to biomarkers listed in Table S2. The map was constructed using Pearson-correlation distance and Ward's linkage rule on means per larval density and after Pareto scaling. Higher than average (mean-centered) values are in red, lower values are in blue.

For each feature, a combination of structural information from Metlin (RRID:SCR_010500), molecular network (MetGem) and public MS/MS databases GNPS (https://gnps.ucsd.edu/ProteoSAFe/libraries.jsp, accessed 12 September 2023) and MS–DIAL (http://prime.psc.riken.jp/compms/msdial/main.html#MSP, accessed 12 September 2023) is proposed (see Figure S7 for five examples of flavonoids). The compound exo-(+)-cinmethylin (n°63, Table S2), a synthetic herbicide and probable environmental contaminant, was discarded, thus reducing the number of putative biomarkers of predation pressure to 207.

Over half of the 207 discriminatory ions implicated in *Buxus* response to predation could be assigned to ten different molecular classes (Fig. 6, Table S2). Involvement of lipid and terpenoid metabolism is especially noticeable, as fatty acyls (six occurrences), steroids (four), mono-, sesqui- and di-terpenoids (1, 5, 6 respectively), triterpenoids (18), and a large number of steroidal alkaloids (37) were annotated. Within the latter class,

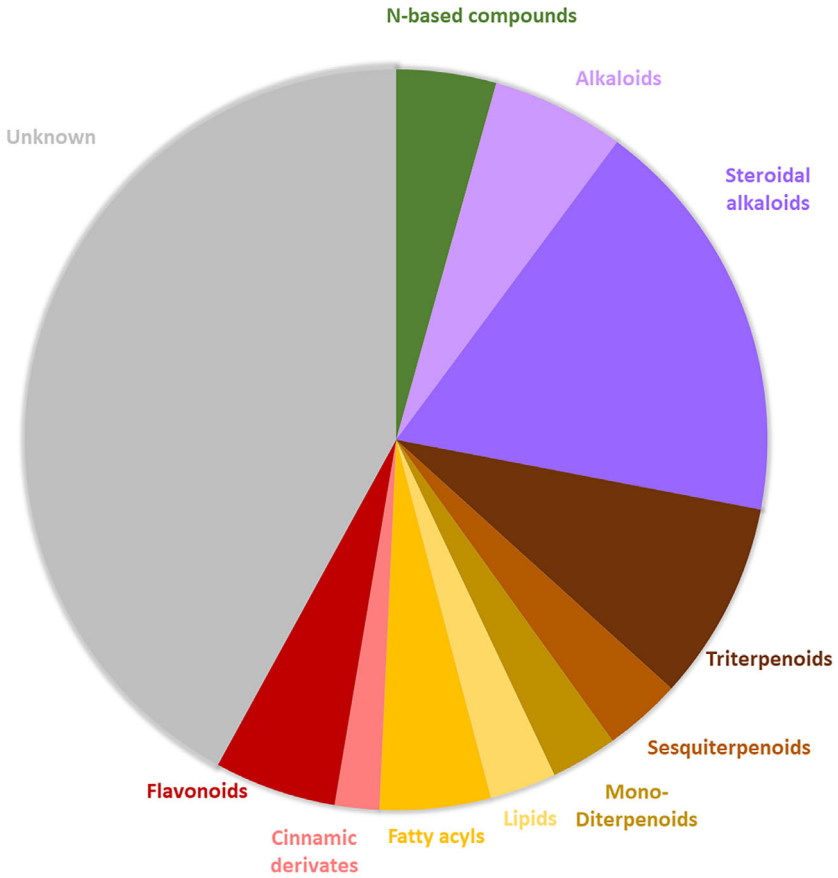

Fig. 6. Repartitioning of 207 most significant LC-MS-based biomarkers selected from *Buxus sempervirens* leaf polar and apolar extracts among different classes of central and specialized metabolisms. Data adapted from Table S2 using the following clustering: N-based compounds contain amino acid derivatives, quaternary ammonium compounds and piperidines; fatty acyls include N-acyl amines; lipids contain steroids, hydroxysteroids and xanthophyll; sesquiterpenoids include hormone derivatives; alkaloids merge benzylisoquinoline, pyrrolizidine, quinolizidine, indole and quinoline alkaloids; cinnamic derivatives contain phenylpropanoids, cinnamaldehydes and cinnamic acids. When appropriate, the same colour code as in Figs 7 and 8 is used.

34 metabolites were previously identified in *Buxus*, e.g. cyclovirobuxine D, buxmicrophylline, buxippine K, cyclobuxophylline O, moenjodaramine. Twelve alkaloids from other biosynthesis pathways also occurred, e.g. (benzyliso)quinoline (derived from tyrosine) and quinolizidine (derived from lysine) alkaloids. A dozen flavonoids (mainly quercetin derivatives and methoxyflavones) and three cinnamic derivatives were also found. In addition, four derivates of carnitine were described.

The heatmap shows metabolic shifts under different predation pressures (Fig. 5C, D). As for central metabolism there was a clear separation delineated for 0.5 predation. The modifications involved all classes of compounds, with emphasis in heatmaps on triterpenoids and alkaloids, whether derived from steroidal or other metabolic pathways. For instance, steroidal alkaloids previously identified in *Buxus* (compounds 116, 120, 122, 163, 178) were overexpressed under high predation pressure, while others (compounds 85, 86, 93, 94, 98, 108, 110, 132) were under-expressed. To confirm the existence of metabolic clusters responding to herbivory pressure and facilitate putative annotation of the most predictive features, we developed molecular networks for LC–MS/MS data of apolar and polar extracts (Figs 7 and 8) using average values for low predation (0–0.25) and high predation (0.5–2.0). Notably, several clusters, developed based on spectral and thus structure similarities, were mainly detected under high herbivory pressure (Figs 7 and 8). A total of 48 ions occurring in both molecular networks are part of a group of 87 recognized as discriminant in box responses but remain unidentified. As examples, cluster AE (2;4) centred on quinolizidine alkaloids, and cluster PE (1;2) centred on indole alkaloids, with accumulation of these substances under high predation. For steroidal alkaloids, positive (AE (2;1), compound 122) or negative (AE (2;1), compounds 85, 96) responses to predation were observed. Flavonoids identified in clusters AE (3;3, compounds 105, 114) and PE (2;14, compounds 201, 207, 208) were more abundant under low predation.

DISCUSSION

Larval predation disrupts central metabolism and induces QAC accumulation in boxwood green leaves

Herbivory effects on plant metabolism have long been investigated, underlining their importance (species identity, kind of herbivore) and intensity of plant–insect interaction (Ali &

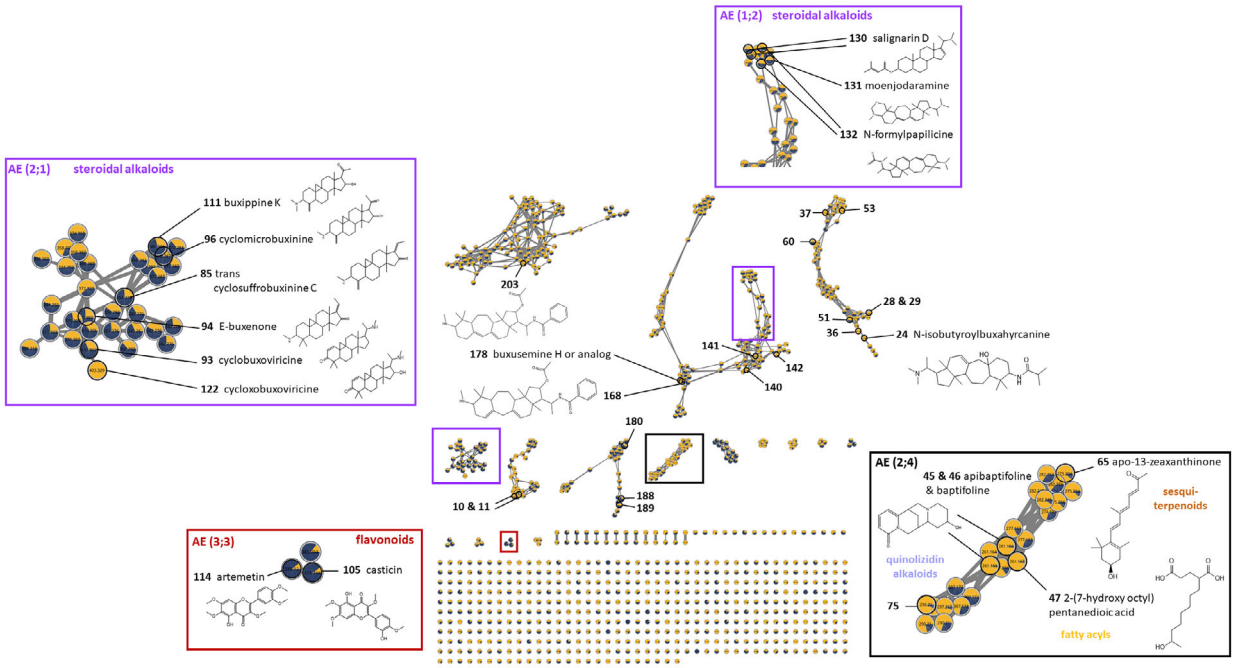

Fig. 7. Molecular networking and details (bold coloured box) of the four clusters AE (1;2), (2;1), (2;4) and (3;3) for apolar extract (AE) of *Buxus sempervirens*, based on 1391 features. Each node represents one feature and the pie chart inside each node refers to relative abundance of the feature. Dark blue nodes indicate no or low predation (mean of four lowest predation pressures, from P = 0 to P = 0.25), and orange nodes indicate high predation (mean of four high predations P = 0.5 to P = 2). Nodes with significant biomarkers have black bold borders. Compound numbers refer to Table S2, some examples of structure of the identified compounds are presented.

Agrawal 2012) for plant responses. For central metabolism, both inhibition and enhancement of fundamental processes of plant growth (*e.g.* photosynthesis and amino acid biosynthesis) have been reported (Zhou *et al.* 2015 for a review) under herbivory. The moth–boxwood interaction is an example of a chewing specialist herbivore feeding on a long-lived and slow-growing plant not adapted to this new pest, despite its large array of defences. Profiling of green leaves reveals consequences of leaf consumption by larvae on central metabolism. Numerous metabolites from different metabolic pathways contribute to shifts in profiles under low predation pressure, followed by major disruption at 0.5 predation pressure, which corresponds to a resource availability of twice the required value.

The progressive decline in glucose and sucrose reflects a possible decrease in leaf photosynthesis. Similarly, photosynthesis of *Tsuga canadensis* needles was negatively affected by attacks by two insects (*Adelges tsugae* and *Firoina externa*; Wilson *et al.* 2018). In carrot leaves (*Daucus carota*) submitted to the carrot psyllid *Bactericerica trigonica*, amounts of photosynthetic pigments decreased proportionally to the increase of nymph density (Othmen *et al.* 2022). The abundance of fructose in leaves can be explained by the specific fructan types (small inulin fructoligosaccharides) described in box leaves (Van den Ende *et al.* 2016) and associated with cold and drought responses. Trehalose in roots could be a similar adaptation: increased predation pressure on leaves caused a decrease in sucrose in roots, which could reflect a collapse of translocation of photosynthetic products to subterranean storage organs.

With the notable exception of Pro, most amino acids accumulated in the remaining green leaves when the plant was attacked, as previously shown for seedlings of *T. canadensis* (Wilson *et al.* 2018). In contrast, Ossipov *et al.* (2014) described a 2.0- to 5.2-fold decrease in four amino acids in *Betula pubescens* leaves damaged by the moth *Epirrita autumnata*, during a 3-year survey. In wounded plants, Asn, a general N-transporter was the dominant amino acid (Figure S2), revealing acute re-organization of central metabolism. Similarly, leaf Asn (and choline) accumulated in 3-year-old *Quercus ilex* as soon as 1 day after wounding (Sardans *et al.* 2014). In the myrmecophyte species *Tococa quadrialata*, Müller *et al.* (2022) found several genes involved in biosynthesis of amino acids (e.g. genes of tryptophan pathway) were induced by ant herbivory, but no clear pattern emerged for protein degradation. In contrast, herbivore-induced shifts in free amino acids have been attributed both to increasing biosynthesis and enhanced proteolysis as a result of insect manipulation of plant gene expression (Zhou *et al.* 2015). Proteolysis is caused by early senescence of cells in attacked leaves in combination with reduced phloem transport. Nitrogen in green leaves is essential to support production of *Buxus* N-based defence metabolites (i.e. alkaloids). In our study, when predation pressure exceeded 0.5 and reached outbreak density, the insects consumed a large portion of the available N, and it is unlikely that the few remaining green leaves could act as an efficient sink.

Between 0 and 0.5 predation pressure, Pro content transiently increased in leaves, in agreement with its role in alleviating environmental stresses (Liang *et al.* 2013) and plant senescence (Szepesi & Szőllősi 2018). When predation pressure became acute, Pro content decreased in leaves (and roots), while other N-containing metabolites, characterized by

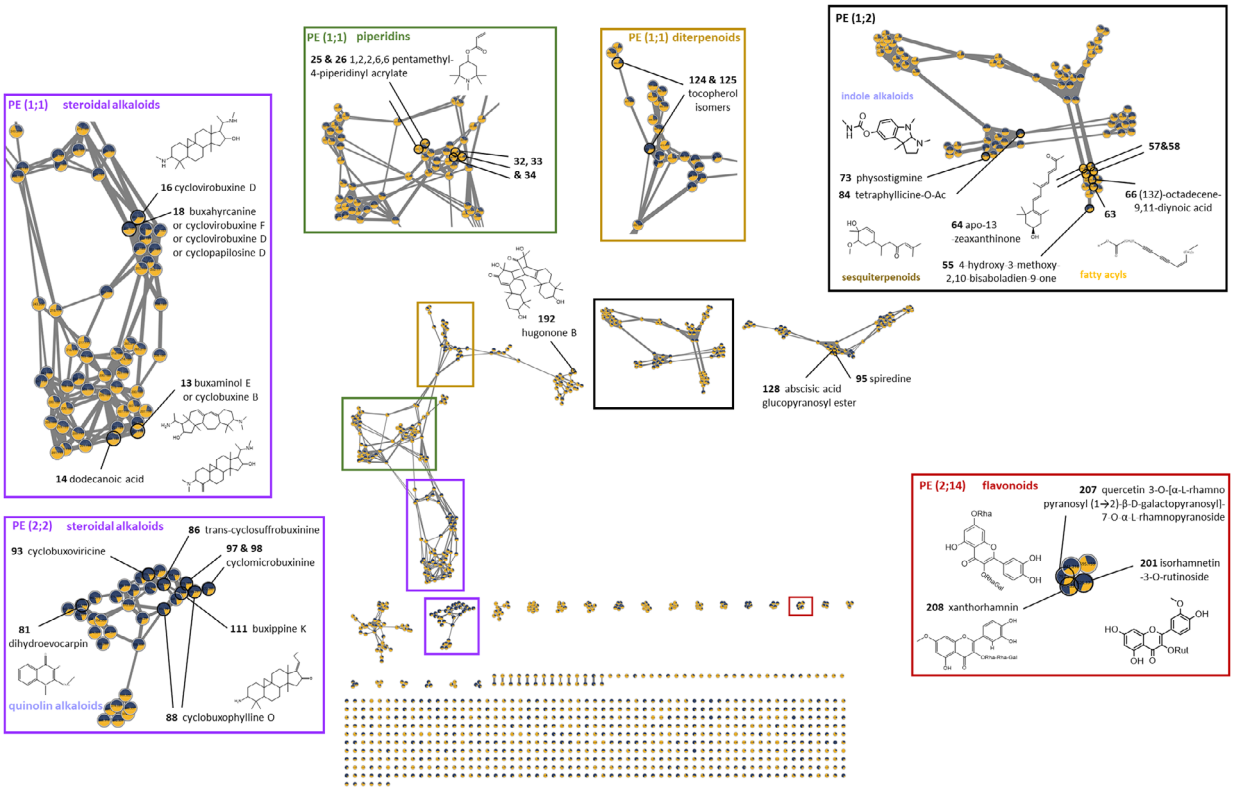

Fig. 8. Molecular networking and details (bold coloured box) of six clusters PE (1;1/3 coloured boxes), (1;2), (2;2), (2;14) for polar extracts (PE), based on 1605 features. Each node represents one feature and the pie chart inside each node refers to relative abundance of the feature. Dark blue nodes indicate no or low predation (mean of four lowest predation pressures from P = 0 to P = 0.25), and orange nodes indicate high predation (mean of four high predations P = 0.5 to P = 2). Nodes with significant biomarkers have bold borders. Compound numbers refer to Table S2, some examples of structure of the identified compounds are presented.

quaternary amines (QACs), tend to accumulate: choline, carnitine, stachydrine and trans–4-hydroxystachydrine; the latter two being proline-derived alkaloids. Among angiosperms, *B. sempervirens* is a high accumulator of less common betaines, trans-4-hydroxystachydrine and stachydrine (Blunden *et al.* 2005). Under herbivory pressures 1.0 or 2.0, trans-4-hydroxystachydrine (10–13% leaf DW) and stachydrine (2–3% leaf DW) were much higher than previously reported, *i.e.* trans-4-hydroxystachydrine 3.2% DW, stachydrine 0.4% DW and trigonelline 0.001% DW (Blunden *et al.* 2005), but without herbivory pressure trans-4-hydroxystachydrine (3.7% leaf DW) and stachydrine (0.7% leaf DW) were similar. These QACs share with Pro a protective role against abiotic stresses as osmolytes implicated in drought protection (Slama *et al.* 2015; Jawahar *et al.* 2019). In our experiment, *Buxus* saplings were watered with natural precipitation, visually monitored and did not suffer from direct drought stress. However, larval damage to vascular tissues and bark of the small saplings probably interrupted sap conduction and produced symptoms similar to those caused by water depletion involving stomatal control (Lin *et al.* 2022). Inositol in leaves and trehalose in roots are other clues for such water stress experienced by *Buxus* saplings. Besides their protective function against abiotic stress, new insights into their roles in plant immunity have been developed both for Pro (Zeier 2013) and other QACs, especially in plant–insect interactions (Ômura 2018). For instance, Pro might be responsible for the feeding preference of gipsy moth (*Lymantrai dispar*) on black poplar leaves, in which increased Pro content was induced. Pro also triggers a phagostimulatory neurone in arctiid moth caterpillars (Bernays *et al.* 2000). Various explanations have been put forward to explain why Pro is favoured by insects, one being that Pro might be an alternative to carbohydrates as fuel for flight, at least in hymenopterans (Teulier *et al.* 2016). Host selection and oviposition are key processes in specialist insect–plant interactions, and oviposition stimulants include Pro and QACs (Honda 1995; Nishida 2014; Ômura 2018). For instance, stachydrine from *Citrus unshiu* leaves is both a larval feeding and oviposition stimulant for swallowtail butterfly (*Papilio xuthus*; Murata *et al.* 2011). In contrast, stachydrine and 3–hydroxystachydrine isolated from *Maerua edulis* have insecticide and anti-oviposition activity towards the cowpea bruchid *Callosobrochus maculatus* (Stevenson *et al.* 2018). It is possible that Pro and/or QACs relative abundance represents an indication of the infestation intensity for boxwood tree moth females. However, further investigations are needed to identify whether Pro, stachydrine and related compounds are involved in oviposition. Nevertheless, existing gaps in complex plant responses to combined abiotic and biotic stress (e.g. drought combined with insect predation) do not exclude cross-involvement of Pro and related compounds (Leisner *et al.* 2023).

Larval predation promotes alkaloid synthesis and diversification

Untargeted metabolomic approaches considering the natural plasticity of *Buxus* specialized metabolites remain recent and rare (Szabó & Schmidt 2022). However, this genus and its impressive cohort of bioactive alkaloids have been surveyed for decades (Athar & Andersh 2008; Xiang *et al.* 2022) because of their medicinal uses (Zhang *et al.* 2015). To our knowledge, no attempt has been made before to link the relative scarcity of predators and parasites that depend on *B. sempervirens* and the richness of its specialized metabolites, especially alkaloids.

Using polar and apolar extracts, we detected over 200 metabolites that are affected by foliar predation by box tree larvae. The flavonoids in *Buxus* leaves, quercetin derivatives and methoxyflavones (casticin and artemetin), are reduced under high herbivory. Importance of phenolic metabolism in tree defence is well known, with numerous phenylpropanoid derivates (*Populus*, *Quercus*, *Salix*, *Betula*; Lämke & Unsicker 2018). *Buxus* constitutive and induced defences depend on increased lipid metabolism, which can be divided into two classes: terpenoids and steroidal alkaloids. The terpenoid class is mainly triterpenoids and, to a lesser extent, by mono-, sesqui- and diterpenoids. Two isomers of tocopherol (delta and gamma) were also detected as putative biomarkers, and the roles of alpha-tocopherol (vitamin E) in regulation of multiple induced responses of birch leaves submitted to *Epirrita autumnata* herbivory was previously described Ossipov *et al.* (2014). Another putative herbivory biomarker related to sterol pathways is apo-13-zeaxanthinone, associated with rare red carotenoids in *Buxus* leaves that offer protection from photoinhibitory conditions during winter (Hormaetxe *et al.* 2005). Lipophilic compounds (triterpenoids, sterols) have already been reported in *Betula pendula* leaves, as a surface defence against larvae of gypsy moth (*Lymantria dispar*) (Martemyanov *et al.* 2015). The thick leaf cuticle of box might also be involved in such defences.

Steroidal alkaloids are mainly synthesized by inclusion of one or two N atoms into a preformed triterpenoid–steroidal pregnane type structure (Athar & Andersh 2008; Xiang *et al.* 2022). Ubiquitous in *Buxus* spp., they also occur mainly in Solanaceae, Liliaceae and Apocynaceae, for which their biological activity has been documented (Bailly 2021). Some respond positively to predation pressure (*e.g.* cycloxobuxoviricine), while others do not (*e.g.* cyclovirobuxine D, buxippine K). More classical alkaloid structures have been identified as biomarkers of moth predation, such as apibaptifoline and baptifoline (quinozilidine alkaloids).

Although our results reinforce the hypothesis of the defence roles of the *Buxus* triterpenoids and alkaloids against insect herbivory, no clear evidence of their repellence or direct toxicity against natural pests exists, as is the case for other species (Bailly 2021). Numerous biological activities have been reported for *Buxus* extracts or molecules, including antiprotozoal (Althaus *et al.* 2014; Szabó *et al.* 2021a,b), antioxidant and enzyme inhibition (Orhan *et al.* 2012), cardioprotection (Xiang *et al.* 2021) activity. Regarding boxwood moth larvae, some adaptation mechanisms were proposed by Leuthardt *et al.* (2013) who showed that larvae growing on *Buxus* leaves can sequester some toxic alkaloids, while others are excreted. The protective role of such sequestration mechanisms against larvae predators (*i.e.* birds) has yet to be demonstrated. Similarly, changes in the volatile profile of box were not investigated here and remain as an open question, while it is tempting to assume that the characteristic scent of *Buxus*, in part from 4-mercapto-methylpentan-2-one (Tominaga & Dubourdieu 1997), could be an important driver of recognition and oviposition in such plant–insect interaction. Changes in plant chemistry must be considered in a multitrophic framework, because direct and indirect chemical defences of *Buxus* are likely to be modified (Gols 2014). For instance, because of the systemic nature of the response, moth invasion can influence plant resistance to other pathogens, like the fungus *Calonectria pseudonaviculata*, another threat to *Buxus* spp. persistence in European stands, or other herbivores. Our results on *B. sempervirens* metabolome responses pave the way to discriminate between resistant and susceptible trees in natural populations, as in *Quercus robur* (Bertić *et al.* 2021).

Central and specialized metabolism are equally influenced by larval density

Our results were obtained on commercial *Buxus* saplings, grown in a mesocosm experiment: this choice was justified by the need to reduce natural genetic variability found in *B. sempervirens* natural populations (Macel & Van Dam 2018), to suppress the influence of soil and environmental parameters and of biotic interactions (mycorrhizae, endophytes, parasites) on the plant metabolome (Schweiger *et al.* 2014). Green leaves that we compared are from shrubs that have undergone very different stresses. We cannot exclude that the remaining green leaves on the most defoliated trees remain because their initial composition made them unpalatable to insects, which could be an alternative explanation for the metabolic differences observed. Having several increasing densities over the critical level of 0.5 pressure reduces the potential importance of this bias.

Under these conditions, we showed that responses of both central and specialized metabolisms after 2 months of predation depend on predation intensity. The shift observed at 0.5 pressure represents the density of larvae where resource availability (= number of *Buxus* leaves) is twice the necessary amount for larval development. Its redundancy as the critical point for metabolism inflexion, whatever the metabolites, highlights the strong connections between central and more specialized biosynthetic pathways. The generalization of this result obtained on a simplified single species interaction involving small *Buxus* trees of commercial origin, to long-lived trees in natural stand, must be viewed with caution.

Even if trees that have been completely defoliated and look dead, some regrowth from the basal part was observed in years following pest invasion in natural stands. The resources needed to build new young twigs and shoots come from the roots and the magnitude of soluble sugar depletion in these organs is probably crucial for this resprouting. The resistance of new shoots to further boxwood moth attack remains to be considered, in light of previous observations of an increase in tree defence compounds in the growing season following severe defoliation. This phenomenon, termed "delayed inducible resistance", seems to depend on tree species and foliage persistence (reviewed by Lämke & Unsicker 2018).

The link between insect density and plant response has rarely been explored, especially using a metabolomics approach. In a natural forested system, Ossipov *et al.* (2014) studied the effect of three different densities of moth as estimated from field visual observations (undamaged, slightly damaged, heavily damaged), but their conclusions on metabolome changes along this limited gradient remain broad.

At the ecosystem level, Belovsky & Slade (2000) demonstrated, by manipulating grasshopper density in the field, that differential herbivory rates have distinct impacts on soil parameters (N availability) through changes in plant litter quality. The magnitude of long-term metabolome variations described here leave little doubt of their ecological consequences. Early senescence of numerous leaves and subsequent massive litterfall following boxwood moth attack have been observed not only in our mesocosm experiment on small saplings, but also in natural stands, causing drastic disruptions compared to normal biogeochemical cycles. The increase in concentrations of various metabolites highlighted in this study should affect litter decomposition rates. Specialized metabolites, especially those based on carbon, can slow biodegradation rates, but little is known about natural biodegradation of alkaloids (Chomel *et al.* 2016). Such adverse effects can be counterbalanced by positive effects represented by the massive N input *via* larval frass, silk and moult produced during moth development (Hunter *et al.* 2012).

Overall, this comprehensive metabolomics study provides the first metabolome depiction of major *Buxus* responses to boxwood moth invasion. As a result, a wider diversity of *B. sempervirens* should be investigated to explore functions of the highlighted compounds, especially derivative alkaloids (trans-4-hydroxystachydrine). Another exciting prospect could be exploring the significance and potential functional redundancy among the wide diversity of boxwood (steroidal) alkaloids.

ACKNOWLEDGEMENTS

We thank A. Chauveau, O. Guillot, A. Dilien and J. Barbe for help in establishment of the *Buxus* mesocosm experiment, and T. Defferier, E. Tabone and A. Bras for providing detailed information on *Cydalima* traits.

AUTHOR CONTRIBUTIONS

A. E. Hay, C. Gallet conceived the experiments. A. Moing, S. Ibanez, L. Ledru, C. Gallet conceived the experimental design. C. Deborde, A. Millery, T. Dussarrat, M. Rey, T. P. T. Hoang, D. Touboul performed the experiments. A. E. Hay, A. Millery, C. Vanhaverbeke, P. Pétriacq, T. Dussarrat analysed the data. A. E. Hay, C. Vanhaverbeke, C. Deborde, T. Dussarrat, C. Gallet wrote the manuscript. All authors reviewed and approved the final manuscript.

FUNDING INFORMATION

This work was supported by University Savoie Mont-Blanc (AAP Recherche 2019); DIPEE Fed. Research Environment Ecology–Zone Atelier Alpes (FA PYRALE, 187) and Metabo-HUB (grant number ANR-11-INBS-0010).

CONFLICT OF INTEREST

The authors declare that they have no conflicts of interest in relation to this work.

DATA AVAILABILITY STATEMENT

NMR data and metadata have been deposited in the recherche.data.gouv.fr repository (https://doi.org/10.57745/HX6NZL) for representative extracts of *B. sempervirens* root and leaf. LC–MS/MS data have been deposited and are available at https://zenodo.org/search?q=touboul&l=list&p=1&s=10&sort=bestmatch.

SUPPORTING INFORMATION

Additional supporting information may be found online in the Supporting Information section at the end of the article.

Figure S1. Experimental design of the mesocosm manipulation.

Figure S2. *B. sempervirens* green leaf content of proteogenic amino acids for the eight increasing *Cydalima* larvae densities.

Figure S3. Stack plots 1D NMR @ 500 MHz of boxwood (A) leaf and (B) root (semi-polar) extracts, for the eight increasing *Cydalima* larvae densities.

Figure S4. (A–C) NMR characterization of stachydrine and trans-4-hydroxystachydrine.

Figure S5. PCA and clustering analysis of ^{1}H-NMR data of *B. sempervirens* roots (central metabolism) along the predation pressure gradient.

Figure S6. Two examples of the chromatograms (LC/MS) obtained from polar (EtOH) and apolar (EToAC) extracts of *B. sempervirens* green leaves.

Figure S7. MS/MS spectrum and mirror plot against standard spectrum for compounds 105, 114, 166, 201, 208.

Table S1. Table of chemical shifts used for identification and quantification of metabolites in 1D ^{1}H-NMR spectra of polar extracts (in deuterated methanol/deuterated phosphate buffer solution, apparent pH 6.0) of *B. sempervirens* leaf and root.

Table S2. List of 208 m/z features detected in polar (PE) and apolar (AE) extracts and identified as biomarkers of *B. sempervirens* leaves.

REFERENCES

Ali J.G., Agrawal A.A. (2012) Specialist versus generalist insect herbivores and plant defense. *Trends in Plant Science*, **17**, 293–302.

Allwood J.W., Williams A., Uthe H., Van Dam N.M., Mur L.A.J., Grant M.R., Pétriacq P. (2021) Unravelling plant responses to stress — The importance of targeted and untargeted metabolomics. *Metabolites*, **11**, 558.

Althaus B.J., Jerz G., Winterhalter P., Kaiser M., Brun R., Schmidt J.T. (2014) Antiprotozoal activity of *Buxus sempervirens* and activity-guided isolation of O-tigloylcyclovirobuxeine-B as the Main constituent active against *Plasmodium falciparum*. *Molecules*, **19**, 6184–6201.

Anzano A., Bonanomi G., Mazzoleni S., Lanzotti V. (2022) Plant metabolomics in biotic and abiotic stress: a critical overview. *Phytochemistry Reviews*, **21**, 503–524.

Athar A., Andersh B.J. (2008) *Buxus* steroidal alkaloids: chemistry and biology. In: Cordell G.A. (Ed), *The alkaloids: chemistry and biology*. Academic Press, London, UK, pp 191–213.

Bailly C. (2021) The steroidal alkaloids α-tomatine and tomatidine: panorama of their mode of action and pharmacological properties. *Steroids*, **176**, 108933.

Barah P., Bones A.M. (2015) Multidimensional approaches for studying plant defence against

insects: from ecology to omics and synthetic biology. *Journal of Experimental Botany*, **66**, 479–493.

Belovsky G.E., Slade J.B. (2000) Insect herbivory accelerates nutrient cycling and increases plant production. *Proceedings of the National Academy of Sciences of the United States of America*, **97**, 14412–14417.

Bernal M., Llorens L., Julkunen-Tiitto R., Badosa J., Verdaguer D. (2013) Altitudinal and seasonal changes of phenolic compounds in *Buxus sempervirens* leaves and cuticles. *Plant Physiology and Biochemistry*, **70**, 471–482.

Bernays E.A., Chapman R.F., Singer M.S. (2000) Sensitivity to chemically diverse phagostimulants in a single gustatory neuron of a polyphagous caterpillar. *Journal of Comparative Physiology A*, **186**, 13–19.

Bertić M., Schroeder H., Kersten B., Fladung M., Orgel F., Buegger F., Schnitzler J.P., Ghirardo A. (2021) European oak chemical diversity – From ecotypes to herbivore resistance. *New Phytologist*, **232**, 818–834.

Blunden G., Patel A.V., Armstrong N., Adrian Romero M., Meléndez P. (2005) Betaine distribution in angiosperms. *Biochemical Systematics and Ecology*, **33**, 904–920.

Bras A., Avtzis D.N., Kenis M., Li H., Vétek G., Bernard A., Courtin C., Rousselet J., Roques A., Auger-Rozenberg M.A. (2019) A complex invasion story underlies the fast spread of the invasive box tree moth (*Cydalima perspectalis*) across Europe. *Journal of Pest Science*, **92**, 1187–1202.

Brockerhoff E.G., Liebhold A.M. (2017) Ecology of forest insect invasions. *Biological Invasions*, **19**, 3141–3159.

Chomel M., Guittonny-Larchevêque M., Fernandez C., Gallet C., DesRochers A., Paré D., Jackson B.G., Baldy V. (2016) Plant secondary metabolites: a key driver of litter decomposition and soil nutrient cycling. *Journal of Ecology*, **104**, 1527–1541.

Davidson C.B., Gottschalk K.W., Johnson J.E. (1999) Tree mortality following defoliation by the European gypsy moth (*Lymantria dispar* L.) in the United States: a review. *Forest Science*, **45**, 74–84.

De Meyer T.P., Sinnaeve D., Van Gasse B., Tsiporkova E., Rietzschel E.R., De Buyzere M.L., Gillebert T.C., Bekaert S., Martins J.C., Van Criekinge W. (2008) NMR-based characterisation of metabolic alterations in hypertension using an adaptive intelligent binning algorithm. *Analytical Chemistry*, **80**, 3783–3790.

Deborde C., Fontaine J.X., Jacob D., Botana A., Nicaise V., Richard-Forget F., Lecomte S., Decourtil C., Hamade K., Mesnard F., Moing A., Molinié R. (2019) Optimising 1D 1H–NMR profiling of plant samples for high throughput analysis: extract preparation standardisation automation and spectra processing. *Metabolomics*, **15**, 28.

Devkota K.P., Lenta B.N., Fokou P.A., Sewald N. (2008) Terpenoid alkaloids of the Buxaceae family with potential biological importance. *Natural Product Reports*, **25**, 612–630.

Di Domenico F., Lucchese F., Magri D. (2012) *Buxus* in Europe: late quaternary dynamics and modern vulnerability. *Perspectives in Plant Ecology, Evolution and Systematics*, **14**, 354–362.

Dyer L.A., Philbin C.S., Ochsenrider K.M., Richards L.A., Massad T.J., Smilanich A.M., Forister M.L., Parchman T.L., Galland L.M., Hurtado P.J. (2018) Modern approaches to study plant–insect interactions in chemical ecology. *Nature Reviews Chemistry*, **2**, 50–64.

Erb M., Reymond P. (2019) Molecular interactions between plants and insect herbivores. *Annual Review of Plant Biology*, **70**, 527–557.

Gols R. (2014) Direct and indirect chemical defences against insects in a multitrophic framework. *Plant, Cell & Environment*, **37**, 1741–1752.

Henderson J., Bicker R., Bidlingmeyer B., Woodward C. (2000) *Rapid accurate sensitive and reproducible HPLC analysis of amino acids: amino acid analysis using Zorbax Eclipse–AAA columns and the Agilent 1100 HPLC*. Agilent Technologies, Application note, Santa Clara, CA, USA.

Honda K. (1995) Chemical basis of differential oviposition by lepidopterous insects. *Archives of Insect Biochemistry and Physiology*, **30**, 1–23.

Hormaetxe K., Becerril J.M., Fleck I., Pintó M., García-Plazaola J.I. (2005) Functional role of red (retro)-carotenoids as passive light filters in the leaves of *Buxus Sempervirens* L.: increased protection of photosynthetic tissues? *Journal of Experimental Botany*, **56**, 2629–2636.

Hunter M.D., Reynolds B.C., Hall M.C., Frost C.J. (2012) Effects of herbivores on terrestrial ecosystem processes: the role of trait-mediated indirect effects. In: Schmitz O., Holt R.D., Ohgushi T. (Eds), *Trait-mediated indirect interactions: ecological and evolutionary perspectives. Ecological reviews*. Cambridge University Press, Cambridge, UK, pp 339–370.

Jawahar G., Rajasheker G., Maheshwari P., Punita D.L., Jalaja N., Kumari P.H., Kumar S.A., Afreen R., Karumanchi A.R., Rathnagiri P., Sreenivasulu N., Kishor P.B.K. (2019) Osmolyte diversity distribution and their biosynthetic pathways. In: Iqbal M., Khan R., Reddy P.S., Ferrante A., Khan N.A. (Eds), *Plant signaling molecules*. Woodhead Publishing, Sawston, UK, pp 449–458.

Kenis M., Auger-Rozenberg M.A., Roques A., Timms L., Péré C., Cock M.J.W., Settele J., Augustin S., Lopez-Vaamonde C. (2009) Ecological effects of invasive alien insects. *Biological Invasions*, **11**, 21–45.

Kenis M., Nacambo S., Leuthardt F.L.G., di Domenico F., Haye T. (2013) The box tree moth *Cydalima perspectalis* in Europe: horticultural pest or environmental disaster? *Aliens: The Invasive Species Bulletin*, **33**, 38–41.

Kuznetsova A., Brockhoff P.B., Christensen R.H.B. (2017) lmerTest package: tests in linear mixed effects models. *Journal of Statistical Software*, **82**, 1–26.

Lämke J.S., Unsicker S.B. (2018) Phytochemical variation in treetops: causes and consequences for tree–insect herbivore interactions. *Oecologia*, **187**, 377–388.

Ledru L., Garnier J., Gallet C., Noûs C., Ibanez S. (2022) Spatial structure of natural boxwood and the invasive box tree moth can promote coexistence. *Ecological Modelling*, **465**, 109844.

Leisner C.P., Potnis N., Sanz-Saez A. (2023) Crosstalk and trade–offs: plant responses to climate change–associated abiotic and biotic stresses. *Plant, Cell & Environment*, **46**, 2946–2963.

Lenth R. 2022. emmeans: estimated marginal means aka Least–squares means. R package version 1.8.1–1. Available from https://github.com/rvlenth/emmeans.

Letts M.G., Rodriguez-Calcerrada J., Rolo V., Rambal S. (2012) Long-term physiological and morphological acclimation by the evergreen shrub *Buxus sempervirens* L. to understory and canopy gap light intensities. *Trees*, **26**, 479–491.

Leuthardt F.L.G., Baur B. (2013) Oviposition preference and larval development of the invasive moth *Cydalima perspectalis* on five European box-tree varieties. *Journal of Applied Entomology*, **137**, 437–444.

Leuthardt F.L.G., Glauser G., Baur B. (2013) Composition of alkaloids in different box tree varieties and their uptake by the box tree moth *Cydalima perspectalis*. *Chemoecology*, **23**, 203–212.

Liang X., Zhang L., Natarajan S.K., Becker D.F. (2013) Proline mechanisms of stress survival. *Antioxidants & Redox Signaling*, **19**, 998–1011.

Lin P.A., Chen Y., Ponce G., Acevedo F.E., Lynch J.P., Anderson C.T., Ali J.G., Felton G.W. (2022) Stomata-mediated interactions between plants herbivores and the environment. *Trends in Plant Science*, **27**, 287–300.

Lopez-Goldar X., Villari C., Bonello P., Borg-Klarson A.K., Zas R., Sampedro L. (2018) Inducibility of plant secondary metabolites in the stem predicts genetic variation in resistance against a key insect herbivore in maritime pine. *Frontiers in Plant Science*, **9**, 1651.

Maag D., Erb M., Glauser G. (2015) Metabolomics in plant–herbivore interactions: challenges and applications. *Entomologia Experimentalis et Applicata*, **157**, 18–29.

Macel M., Van Dam N.M. (2018) Metabolomics of plant resistance to insects. In: Emani C. (Ed), *The biology of plant–insect interactions*. CRC Press, Boca Raton, FL, USA, pp 129–149.

Martemyanov V.V., Pavlushin S.V., Dubovskiy I.M., Belousova I.A., Yushkova Y.V., Morosov S.V., Chernyak E.I., Glupov V. (2015) Leaf surface lipophilic compounds as one of the factors of silver birch chemical defense against larvae of gypsy moth. *PLoS One*, **10**, e0121917.

Mitchell R., Chitanava S., Dbar R., Kramarets V., Lehtijärvi A., Matchutadze I., Mamadashvili G., Matsiakh I., Nacambo S., Papazova-Anakieva I., Sathyapala S., Tuniyev B., Vétek G., Zukhbaia M., Kenis M. (2018) Identifying the ecological and societal consequences of a decline in *Buxus* forests in Europe and the Caucasus. *Biological Invasions*, **20**, 3605–3620.

Müller A.T., Nakamura Y., Reichelt M., Luck K., Cosio E., Lackus N.D., Gershenzon J., Mithöfer A., Köllner T.G. (2024) Biosynthesis, herbivore induction, and defensive role of phenylacetaldoxime glucoside. *Plant Physiology*, **194**, 329–346.

Müller A.T., Reichelt M., Cosio E.G., Salinas N., Nina A., Wang D., Moossen H., Geilmann H., Gershenzon J., Köllner T.G., Mithöfer A. (2022) Combined -omics framework reveals how ant symbionts benefit the Neotropical ant-plant *Tococa quadrialata* at different levels. *iScience*, **25**, 105261.

Murata T., Mori N., Nishida R. (2011) Larval feeding stimulants for a Rutaceae-feeding swallowtail butterfly *Papilio xuthus* L. in *Citrus unshiu* leaves. *Journal of Chemical Ecology*, **37**, 1099–1109.

Nishida R. (2014) Chemical ecology of insect–plant interactions: ecological significance of plant secondary metabolites. *Bioscience Biotechnology and Biochemistry*, **78**, 1–13.

Olivon F., Grelier G., Roussi F., Litaudon M., Touboul D. (2017) MZmine 2 data-preprocessing to enhance molecular networking reliability. *Analytical Chemistry*, **89**, 7836–7840.

Ômura H. (2018) Plant secondary metabolites in host selection of butterfly. In: Tabata J. (Ed), *Chemical ecology of insects: applications and associations with plants and microbes*. CRC Press, Boca Raton, FL, USA, pp 3–27.

Orhan I.E., Erdem S.A., Senol F.S., Kartal M., Sener B. (2012) Exploration of cholinesterase and tyrosinase

inhibitory antiprotozoal and antioxidant effects of *Buxus sempervirens* L. (boxwood). *Industrial Crops and Products*, **40**, 116–121.

Ossipov V., Klemola T., Ruohomäki K., Salminen J.P. (2014) Effects of three years' increase in density of the geometrid *Epirrita autumnata* on the change in metabolome of mountain birch trees (*Betula pubescens* ssp. *czerepanovii*). *Chemoecology*, **24**, 201–214.

Othmen B.S., Boussaa F., Hajji-Hedfi L., Abbess K., Dbara S., Chermiti B. (2022) Effects of nymphal density (*Bactericera trigonica*) and feeding on photosynthetic pigments proline content and phenolic compounds in carrot plants. *European Journal of Plant Pathology*, **163**, 51–59.

Sanchez-Arcos C., Kai M., Svatos A., Gershenzon J., Kunert G. (2019) Untargeted metabolomics approach reveals differences in host plant chemistry before and after infestation with different pea aphid host races. *Frontiers in Plant Science*, **10**, 188.

Sardans J., Gargallo-Garriga A., Pérez-Trujillo M., Parella T.J., Seco R., Filella I., Peñuelas J. (2014) Metabolic responses of *Quercus ilex* seedlings to wounding analysed with nuclear magnetic resonance profiling. *Plant Biology*, **16**, 395–403.

Schweiger R., Heise A.M., Persicke M., Müller C. (2014) Interactions between the jasmonic and salicylic acid pathway modulate the plant metabolome and affect herbivores of different feeding types. *Plant, Cell & Environment*, **37**, 1574–1585.

Slama I., Abdelly C., Bouchereau A., Flowers T., Savouré A. (2015) Diversity distribution and roles of osmoprotective compounds accumulated in halophytes under abiotic stress. *Annals of Botany*, **115**, 433–447.

Stevenson P.C., Green P.W.C., Farrell L.W., Brankin A., Mvumi B.M., Belmain S.R. (2018) Novel Agmatine derivatives in *Maerua edulis* with bioactivity against *Callosobruchus maculatus* a cosmopolitan storage insect Pest. *Frontiers in Plant Science*, **9**, 1506.

Sumner L.W., Amberg A., Barrett D., Beale M.H., Beger R., Daykin C.A., Fan T.W.-M., Fiehn O., Goodacre R., Griffin J.L., Hankemeier T., Hardy N., Harnly J., Higashi R., Kopka J., Lane A.N., Lindon J.C., Marriott P., Nicholls A.W., Reily M.D., Thaden J.J., Viant M.R. (2007) Proposed minimum reporting standards for chemical analysis. *Metabolomics*, **3**, 211–221.

Szabó L.U., Kaiser M., Mäser P., Schmidt T.J. (2021a) Antiprotozoal nor-triterpene alkaloids from *Buxus sempervirens* L. *Antibiotics*, **10**, 696.

Szabó L.U., Kaiser M., Mäser P., Schmidt T.J. (2021b) Identification of antiprotozoal compounds from *Buxus sempervirens* L. by PLS-prediction. *Molecules*, **26**, 6181.

Szabó L.U., Schmidt T.J. (2022) Investigation of the variability of alkaloids in *Buxus sempervirens* L. using multivariate data analysis of LC/MS profiles. *Molecules*, **27**, 82.

Szepesi A., Szőllősi R. (2018) Mechanism of Proline biosynthesis and role of Proline metabolism enzymes under environmental stress in plants. In: Ahmad P., Ahanger M.A., Singh V.P., Tripathi D.K., Alam P., Alyemeni M.N. (Eds), *Plant metabolites and regulation under environmental stress*. Academic Press, London, UK, pp 337–353.

Teulier L., Weber J.M., Crevier J., Darveau C.A. (2016) Proline as a fuel for insect flight: enhancing carbohydrate oxidation in hymenopterans. *Proceedings of the Royal Society B: Biological Sciences*, **283**, 20160333.

Tominaga T., Dubourdieu D. (1997) Identification of 4-mercapto-4-methylpentan-2-one from the box tree (*Buxus sempervirens L.)* and broom (*Sarothamnus scoparius* (L.) Koch). *Flavour and Fragrance Journal*, **12**, 373–376.

Van den Ende W., Coopman M., Vergauwen R., Van Laere A. (2016) Presence of inulin-type Fructo-oligosaccharides and shift from Raffinose family oligosaccharide to Fructan metabolism in leaves of Boxtree (*Buxus sempervirens*). *Frontiers in Plant Science*, **7**, 209.

Van der Straten M.J., Muus T.S.T. (2010) The box tree pyralid *Glyphodes perspectalis* (Lepidoptera: Crambidae), an invasive alien moth ruining box trees. *Proceedings of the Netherlands Entomological Society*, **21**, 107–111.

Wilson C.M., Schaeffer R.N., Hickin M.L., Rigsby C.M., Sommi A.F., Thornber C.S., Orians C.M., Preisser E. (2018) Chronic impacts of invasive herbivores on a foundational forest species: a whole-tree perspective. *Ecology*, **99**, 1783–1791.

Xiang M.L., Hu B.Y., Qi Z.H., Wang X.N., Xie T.Z., Wang Z.J., Ma D.Y., Zeng Q., Luo X.D. (2022) Chemistry and bioactivities of natural steroidal alkaloids. *Natural Products and Bioprospecting*, **12**, 23.

Xiang Z.N., Su J.C., Liu Y.H., Deng B., Zhao N., Pan J., Hu Z.F., Chen F.H., Cheng B.Y., Chen J.C., Wan L.S. (2021) Structurally diverse alkaloids from *Buxus sempervirens* with cardioprotective activity. *Bioorganic Chemistry*, **109**, 104753.

Zeier J. (2013) New insights into the regulation of plant immunity by amino acid metabolic pathways. *Plant, Cell & Environment*, **36**, 2085–2103.

Zhang J., Qin X.Y., Zhang S.D., Xu X.S., Pei J.P., Fu J.J. (2015) Chemical constituents of plants from the genus *Buxus*. *Chemistry and Biodiversity*, **12**, 1289–1306.

Zhou S., Lou Y.R., Tzin V., Jander G. (2015) Alteration of plant primary metabolism in response to insect herbivory. *Plant Physiology*, **169**, 1488–1498.